Nanotechnology

Alkali-resistant low-temperature atomic-layer-deposited oxides for optical fiber sensor overlays

To cite this article before publication: Kamil Kosiel *et al* 2018 *Nanotechnology* in press https://doi.org/10.1088/1361-6528/aaa9a3

Alkali-resistant low-temperature atomic-layer-deposited oxides for optical fiber sensor overlays

K Kosiel[1], M Dominik[2], I Ściślewska[2], M Kalisz[3], M Guziewicz[1], K Gołaszewska[1], J Niedziółka-Jonsson[4], W J Bock[5] and M Śmietana[2]

[1] Instytut Technologii Elektronowej, Al. Lotników 32/46, 02-668 Warsaw, Poland
[2] Institute of Microelectronics and Optoelectronics, Faculty of Electronics and Information Technology, Warsaw University of Technology, Koszykowa 75, 00-662 Warsaw, Poland
[3] Motor Transport Institute, Jagiellońska 80, 03-301 Warsaw, Poland
[4] Institute of Physical Chemistry, Polish Academy of Sciences, Kasprzaka 44/52, 01-224 Warsaw, Poland
[5] Centre de recherche en photonique, Université du Québec en Outaouais, 101 rue Saint-Jean-Bosco, Gatineau, QC J8X 3X7, Canada
e-mail: kkosiel68@gmail.com, kosiel@ite.waw.pl

Abstract: The paper presents investigation of properties of selected metallic oxides deposited at low temperature (100°C) by atomic layer deposition (ALD) technique, relating to their applicability as thin overlays for optical fiber sensors resistant in alkaline environments. Hafnium oxide (Hf_xO_y with y/x approx. 2.70), tantalum oxide (Ta_xO_y with y/x approx. 2.75) and zirconium oxide (Zr_xO_y with y/x approx. 2.07), which deposition was based, respectively, on tetrakis(ethylmethyl)hafnium, tantalum pentachloride and tetrakis(ethylmethyl)zirconium with deionized water, were tested as thin layers on planar Si (100) and glass substrates. Growth per cycle (GPC) in the ALD processes was 0.133-0.150 nm/cycle. Run-to-run GPC reproducibility of the ALD processes was best for Hf_xO_y (0.145±0.001 nm/cycle) and the poorest for Ta_xO_y (0.133±0.003 nm/cycle). Refractive indices *n* of the layers were 2.00-2.10 (at the wavelength λ=632 nm), with negligible *k* value (at λ for 240-930 nm). The oxides examined by x-ray diffractometry proved to be amorphous, with only small addition of crystalline phases for the Zr_xO_y. The surfaces of the oxides had grainy but smooth topographies with root-mean square roughness ~0.5 nm (at 10×10 μm^2 area) according to atomic force microscopy. Ellipsometric measurements, by contrast, suggest rougher surfaces for the Zr_xO_y layers. The surfaces were also slightly rougher on the glass-based samples than on the Si-based ones. Nanohardness and Young modules were 4.90-8.64 GPa and 83.7-104.4 GPa, respectively. The tests of scratch resistance revealed better tribological properties for the Hf_xO_y and the Ta_xO_y than for the Zr_xO_y. The surfaces were hydrophilic, with wetting angles of 52.5-62.9°. The planar oxides on Si, being resistive even to concentrated alkali (pH 14), proved to be significantly more alkali-resistive than Al_2O_3. The Ta_xO_y overlay was deposited on long-period grating sensor induced in optical fiber. Thanks to such an overlay the sensor proved to be long-lasting resistant when exposed to alkaline environment with a pH 9. Thereby, it also proved that it has a potential to be repeatedly reused as a regenerable optical fiber biosensor.

Keywords: optical fiber sensors, thin film overlays, Atomic Layer Deposition, alkali-resistant materials, long-period gratings
PACS: 42.81.Pa, 42.79.Wc, 81.15.Gh, 81.70.Fy, 78.20.Ci, 42.70.Ce, 68.55.jd, 68.55.J 68.37.Ps

1. Introduction

The field of optical sensors covers a wide range of device architectures, physical effects and sensing strategies. When for example optical fiber devices are concerned, different structures or their modifications may be used in order to promote interaction of light with the analysed external environment, such as, e.g., fiber Bragg gratings (FBGs), long-period gratings (LPGs) [1], fiber tapers, or fiber heterostructures [2-4].

Novel optical sensors the most often require thin films or surface structures with different properties that initiate or modify sensorial response of these devices. These nano-materials may be metallic as in case of surface plasmon resonance (SPR) or localized surface plasmon resonance (LSPR) or show dielectric properties as in case of lossy mode resonance (LMR) phenomenon [5]. Sensing properties of these devices strongly depend on properties of these thin film materials, such as their electrical permittivity or optical properties and size or thickness. It has been shown that couple of nanometres difference in size has a strong influence on response of the device and may drastically change its sensing performance [6]. This fact places stringent requirements on control of the appropriate size of the nanostructures, or thickness of the layer and their optical properties.

Apart from the mentioned above properties determining the sensorial response, these materials are the most external. Because of this, they should also be resistant to environmental threats or even they should play a role of protective coatings for vulnerable sensors. That is why it is expected from the mentioned materials to show high hardness and chemical corrosion resistance. These properties of the nanostructures are necessary for sensor application in harsh environment measurements, which can include strong alkaline solutions. The most often used material for fabrication of optical fibers is fused silica, which is also corrosive in hot concentrated alkali solutions [7]. This fact confirms the usefulness of appropriately protective coatings. Some industrial processes, such as gold plating, are performed in high-pH solutions. Therefore there is a technical need for strict chemical control of such solutions, like for example for control of oxygen concentration in the case of plating. Most of commercially available sensors, however, are not applicable for pH greater than 9 [8]. Apart from the matter of measurements performed in alkali, also the process of biosensor regeneration that allows for its reusability, may require treatment in high-pH alkaline solutions. An example of this is a regeneration process of specific TiO_2-overlaid optical fiber biosensors with silane-functionalized active surfaces, for which a solution with a pH 14 was applied [9, 10]. Although such high pH value was not optimized and in further experiments it was confirmed that already the pH equal to 9 worked effectively for the sensor regeneration process [11], the alkali treatment still remains necessary.

The dielectric materials that are most commonly used as thin overlays in optical sensors are oxides. Aluminium oxide (Al_2O_3) [12], titanium dioxide (TiO_2) [13, 14], tin dioxide (SnO_2) [15], indium (III) oxide (In_2O_3) [16], and indium-tin oxide (ITO) [17-22] are most often used for this purpose. Polymeric thin films, like polyallylamine hydrochloride/polyacrylic acid (PAH/PAA) films are also used [23]. However, most of the overlay materials are not resistant to chemicals, in particular to strong alkali solutions. For example Al_2O_3 and SnO_2 are vulnerable to degradation in alkaline solutions because of their amphoteric chemical nature [24]. Probably for the same reason also TiO_2 layers are not totally safe during prolonged stay in alkali [9, 10, 25], and they may dissolve very slowly.

The thin overlays used to be deposited mostly by Langmuir-Blodgett method [1], spin coating [26], sol-gel process [27], layer-by-layer technique [28], chemical vapour deposition (CVD) [29], or physical vapour deposition (PVD) methods, which include evaporation [30] or sputtering [31]. These methods, however, have specific drawbacks especially when it comes to deposition of nanolayers on nonplanar surfaces, such as on the surfaces of optical fibers. The drawbacks may generally relate to facility of overlay thickness control – uniformity, conformity, accuracy, repeatability, spatial resolution - or to mechanical and thermal stability of the layers. The chemical precursor availability or available growth rates may also be an important issue.

The atomic layer deposition (ALD) technique is a very special variation of CVD method, in which the chemical precursors are delivered to the reaction zone separately in a real time [32]. It is crucial that the complementary and sequentially repeated chemical reactions responsible for the layer growth undergo at a surface in a self-limiting manner. Thanks to this paradigm, an atomic control of the layer thickness is possible, with uniquely conformal and uniform layers, even when they are

deposited on complicated high-aspect-ratio surfaces. The ALD-deposited high quality layers are tight and dense, and may show various optical properties as requested by optical sensors. The ALD technique enables deposition of a wide range of materials – oxide isolators, semiconductors and conductors, nitride isolators and semiconductors, metallic nitrides, II-VI semiconductors and luminescent materials, III-V semiconductors, metals and many others [32]. This is the reason why the ALD technique is a must in nowadays microelectronics [33, 34], but at the same time it reaches more and more applications in other very divers branches [35, 36]. It has also been used in optical sensors technology for a few years [9, 10, 37-40]. It should be emphasized here that ALD allows for deposition at relatively low temperatures (LT), even much below 100°C, that is an important advantage in comparison with the continuous-CVD method, especially when taking into account relatively low thermal stability of many optical sensor devices.

Generally, the composition of as-deposited oxides of hafnium, zirconium and tantalum may be complicated. There can exist pure stoichiometric forms, mixtures of stoichiometric forms [41], and non-stoichiometric oxides (including suboxides, e.g. hafnium suboxide [42], as well as "overstoichiometric" compositions, e.g. "overstoichiometric" tantalum oxide [43]). There are well known HfO_2 and ZrO_2 stoichiometric oxides [44]. There are also known relatively stable monoxides of Hf and Zr [45]. The tantalum stoichiometric oxides comprise compounds of tantalum with various oxidation states between +2 and +5, like TaO, Ta_2O_3, TaO_2 and Ta_2O_5. The most thermodynamically stable state of tantalum in oxides is +5 [46, 47].

The stoichiometric HfO_2 is a material that for several years has widely been deposited by ALD technique, mainly as a high dielectric constant (high-*k*) isolator in microelectronics industry [48, 49]. HfO_2 was also reported in the literature of optical sensors [50]; however, on the basis of literature data, one might suppose lack of stability of HfO_2 in very strong bases [51, 52]. Also stoichiometric ZrO_2 and Ta_2O_5 are relatively widely used as microelectronic high-*k* dielectrics [33, 53], and they also can be deposited by ALD. They are well known for their general low chemical reactivity [54] and hence they may be expected to be stable in alkali. Ta_2O_5 has already been reported as a material for evanescent field sensors [31].

In this work we critically considered applicability of selected metallic oxides, in terms of facility for convenient deposition by LT-ALD in the form of nanooverlays matching the optical fiber sensor technology requirements, testing at the same time if they were capable to ensure the sensor robustness in alkali up to harsh environments (pH 14). The tested oxides were: hafnium oxide (Hf_xO_y with y/x of approx. 2.70), zirconium oxide (Zr_xO_y with y/x of approx. 2.07, i.e. very close to the stoichiometric ZrO_2) and tantalum oxide (Ta_xO_y with y/x of approx. 2.75). It should be highlighted here that the just-reported y/x values relate to the investigated Hf_xO_y, Zr_xO_y and Ta_xO_y, wherever these materials are mentioned within the entire article. It should be noted as well that in contrast to the nearly stoichiometric composition of the deposited Zr_xO_y, the obtained Hf_xO_y and Ta_xO_y were clearly "overstoichiometric". Study of compositions of the oxides, performed using Rutherford backscattering spectroscopy (RBS) and x-ray photoelectron spectroscopy (XPS), is a subject of separate articles - therefore, it is not described here.

2. Experimental Details

Our initial tests of chemical robustness in alkali were performed by using planar test layers of the oxides as a model. After that test, the tribological, structural, topographical and hydrophilic properties were studied for the promising oxide layers. These properties are important for sensor-overlay applications. Basic properties of the relevant ALD-growth processes were also described. The selected oxide overlay was deposited on the optical fibers with induced LPGs in order to check the stability of spectral response of such sensors when exposed to alkaline environment. From this experiment the conclusion on chemical stability of the oxide overlay in alkali was also drawn. In a LPG-based fiber sensor its sensorial properties are induced by refractive index *n* modulation in the optical fiber core while the overlay modifies the sensorial response and allows for its appropriate adjustment according to the need. The LPG-based sensor structure was chosen for this test, because its spectral response is widely known as being strongly dependent on thickness and refractive index of its thin overlay [1, 40]. It is likely that even subnanometre thickness changes of the overlay should be detectable in this case. We also compared stability of the studied oxides with Al_2O_3. This oxide is

probably the most popular ALD-deposited material [55, 56], and at the same time it is very often used in technique of optical sensors [12, 40], though, as it was mentioned above, Al_2O_3 is amphoteric and hence it is strongly presumed soluble in alkaline solutions. Here, we decided to refer to the ALD-deposited Al_2O_3 behaviour in alkali in order to make this point clear in quantitative terms.

2.1. ALD processes

The ALD processes were performed, using Beneq TFS-200-190 system [57]. The system is equipped with a flow reaction chamber with dimensions 200×3 mm (diameter and height, respectively). The ALD was performed in thermal mode at the thermocouple-controlled reactor temperature 100±0.1°C. Such LT of the process was unavoidable because of the thermal vulnerability of a polymer coating that optical fibers are originally covered by. Moreover, the refractive index modulation in the LPG structures is vulnerable in a special way, as the permanent inhomogeneous space-charge distribution and the related internal electric field – being the cause of the index modulation – would be destroyed by high temperature. Additionally, LT enables deposition of amorphous layers and hence smoother surfaces (than for the polycrystalline forms), which are preferred for the purpose of more uniform layer thickness achievement as well as for suppression of light scattering. The carrier/purging gas was 6N-purity argon (Ar), which flow through the reactor was kept at 600 sccm for the Al_2O_3 deposition and at 1000 sccm for the other oxides. The Ar pressure inside the reactor was ~2 mbar. Trimethylaluminium (TMA) and deionized water (DI H_2O), both kept at 19±0.1°C in Beneq's standard LS containers, were used as chemical precursors for aluminium and oxygen, respectively. Tantalum pentachloride ($TaCl_5$, kept at 85±0.1°C), tetrakis(ethylmethylamino)zirconium (TEMAZ, kept at 75±0.1°C), and tetrakis(ethylmethylamino)hafnium (TEMAH, kept at 78±0.1°C), all kept in Beneq's standard HS 300 containers, were used as chemical precursors for tantalum, zirconium and hafnium, respectively. The equations (1)-(4) present the total effect of chemical reactions occurring at the growing surfaces during ALD processes based on the mentioned above precursors. The symbol (g) and the symbol (s) in the equations refer to the chemical species in a gas phase and in a solid phase, respectively. The equations are given for the stoichiometric forms of oxides - Al_2O_3 (eq. 1), HfO_2 (eq. 2), ZrO_2 (eq. 3), Ta_2O_5 (eq. 4). Therefore, in the case of "overstoichiometric" forms one should take into account the incorporation of additional amounts of oxygen.

$$Al(CH_3)_3\,(g) + 3/2\ H2O\ (g) \rightarrow 1/2\ Al_2O_3\,(s) + 3CH_4\,(g) \quad (1)$$

$$Hf(N(C_2H_5)(CH_3))_4\,(g) + 2\ H_2O\ (g) \rightarrow HfO_2\,(s) + 4\ HN(C_2H_5)(CH_3)\,(g) \quad (2)$$

$$Zr(N(C_2H_5)(CH_3))_4\,(g) + 2\ H_2O\ (g) \rightarrow ZrO_2\,(s) + 4\ HN(C_2H_5)(CH_3)\,(g) \quad (3)$$

$$8\ TaCl_5\,(g) + 20\ H_2O\ (g) \rightarrow 4Ta_2O_5\,(s) + 10HCl\,(g) \quad (4)$$

Deposition of the layers was performed on two kinds of planar substrates - glass plates and (100)-oriented silicon (Si) wafers. Selected ALD processes were performed also for optical fibers. The planar samples were intended for analyses that could not be performed using fiber samples. The surface of the glass plate was supposed to be more similar to the surface of the silica fiber than the surface of Si. The similarity is assumed in terms of surface density of functional groups being the chemically active centers in ALD process. Therefore, whenever possible, the glass-based samples were used for analyses. On the other hand, the spectroscopic ellipsometry (SE) measurements on the glass-based samples were too problematic, as the multiple reflections make the fitting process ambiguous. Therefore the Si-based samples were used whenever the SE was involved. The Si wafers (manufactured by Topsil Semiconductors sp. z o.o.) were p-type doped with electrical resistivity of approx. 3-5 Ωcm. They had typically dimensions of a quarter of 4-inch-diameter wafer. The glass plates were rectangular-shaped, with dimensions 76×26×1 mm. Planar substrates were not subjected to any pre-treatment before the ALD processes. The fibers were fused-silica-based with induced LPGs.

LPGs were induced in hydrogen-loaded germanium-doped using UV laser irradiation and chromium mask with period of 226.8 μm [40]. The excess of hydrogen has been released after the irradiation by sample annealing for 4h in 150°C. The Corning SMF28 optical fiber was used for sensor fabrication. The fiber geometry is cylindrical. Its cladding and jacket (original protective coating) diameter is 125±0.7 μm and 242±5 μm, respectively. The active region of the sensor was fabricated over a distance of tens of mm, where the jacket was removed exposing the cladding. The LPG pattern was fabricated inside the waveguide core, within the stripped fiber fragment. The stripped fiber fragment was coated by the ALD overlay. Before entering the ALD reactor the fibers were rinsed with acetone and isopropanol at the ambient temperature (approx. 20°C). All kinds of the substrates were positioned in a run-to-run-repeatable manner inside the ALD reactor. The curved edges of Si quarters were positioned at a distance of approx. 50 mm from the gas inlet.

The precursor exposures were experimentally determined already before the experiments described in this paper. The exposures ensured substrate-surface-saturation conditions for all complementary chemisorption half reactions involved in the employed ALD processes. On this basis the appropriate precursor/purge-cycling schemes were determined. They were studied using Si substrates, and they are not described here. For the optimized cycling conditions the growth per cycle (GPC) measured for Si-based samples was 0.099, 0.133, 0.15 and 0.145 nm/cycle for the Al_2O_3, Ta_xO_y, Zr_xO_y and Hf_xO_y layer, respectively. The resulting layer growth rate was 0.02, 0.019, 0.022, and 0.021 nm/s for the Al_2O_3, Ta_xO_y, Zr_xO_y and Hf_xO_y, respectively. The thickness range of the layers investigated in this paper was 32-210 nm, as confirmed by *ex-situ* SE.

2.2. Characterization of the oxides

The chemical resistance of the planar oxide layers was tested by immersion the approx. 2 cm^2-large Si-based samples in 1 M NaOH aqueous solution (pH 14) at the ambient temperature (approx. 20°C). The pH value was measured by a pH strip before each immersion. The solution was prepared by dissolution of analytical grade granular NaOH (delivered by Avantor Performance Materials Poland S.A.) in DI water. In the alkaline stability tests the static conditions of the bath were maintained. Because the tested samples were planar without any fabricated surface topography/pattern it was not found necessary to apply circulation in the bath. The test results were confirmed by using at least two samples for each kind of oxide. After each immersion, performed for controlled time duration, the sample was rinsed in DI water and dried with compressed nitrogen. Then, the stability of its thickness was examined by SE method. The measurements were performed in a set of positions (points) adjusted manually on the sample surface. The measurement positions were fixed for the whole experiment (repeatedly used in successive measurements after immersions). The spatial pattern of the positions was the same for each sample. In each position three SE measurements were done after each immersion. The mean value of thickness in each position was calculated assuming normal distribution and 95% confidence interval. On this basis the thickness stability was checked after each immersion. Each sample was alkali-treated in this way according to the following scheme of multiple immersion: 5 min-lasting immersion (for two consecutive repeats), 2 h-lasting immersion, and 20 h-lasting immersion. The longer immersions were applied only when the shorter tests were successfully passed.

The thicknesses and complex refractive indices of the layers were analysed by SE using Sentech SE800E spectrometer. Measurements were performed at the ambient conditions, at the temperature of approx. 20°C, in the spectral range of 240-930 nm for 50, 60 and 70° beam incident angles. The measurement results were fitted by using the sample structure models that proved to ensure the best quality of fit parameters, using the χ^2 parameter optimisation procedure. The χ^2 parameter values were typically below unity. Therefore, Tauc-Lorentz, Sellmeier, Tauc-Lorentz and Cauchy models [58] were applied for fitting the Al_2O_3, Ta_xO_y, Zr_xO_y and Hf_xO_y-based samples, respectively. The parametrised control of fit quality shows that these models, though calibrated for stoichiometric compounds, have worked also for our overstoichiometric layers. The Zr_xO_y layers were best fitted when certain surface roughness was assumed, formally included to the ZrO_2-sample model as an additional topmost effective medium approximation (EMA) layer. Because the native SiO_2 was not removed from the Si wafers before ALD processes, the presence of 2 nm-thick SiO_2 interfacial layer was assumed in ellipsometric models (with the real part of refractive index n=1.46 and negligible

imaginary part of refractive index *k*). The respective optical properties of native SiO_2 were earlier found in SE measurements of the bare Si wafers.

The structural properties of the glass-based 50-65 nm-thick as well as approx. 200 nm-thick layers were investigated by XRD (x-ray diffractometry) technique using X'Pert Empyrean PANalytical equipment equipped with Cu K-alpha radiation source, the Johanson's filter and PIXcel2D detector. The theta-2theta scans were performed at ambient conditions. Surface topographies were analysed by AFM (atomic force microscopy) technique using Veeco diInnova equipment for the 50-60 nm-thick glass-based layers and compared with the Si-based ones. The measurements were performed using tapping mode in air at the ambient temperature approx. 20°C, by scanning the areas of 2x2 μm^2 as well as 10x10 μm^2, with resolution of 512 lines per scan, and with horizontal scan rate 0.5 Hz.

The Attension Theta Lite optical tensiometer was used to evaluate DI water contact angles of the layers, according to the sessile drop method [59]. This was a test of surface hydrophilicity.

The approx. 200 nm-thick glass-based layers were used for nanohardness (H_{it}) and elasticity (Young moduli, E_{it}) measurements - performed using the CSM Instrument (Peseux, Switzerland) nanoindenter equipped with Vickers diamond indenter - as well as for abrasion resistance tests - performed using a Summers Optical's Lens Coating Hardness Test Kit (EMS Acquisition Corp., USA). Details underlying the used nanoindentation-based characterization methods have already been comprehensively presented elsewhere [60-62]. The abrasion resistance tests were performed according to the well-acknowledged standard [63] and literature reports [64]. The surfaces were examined by an optical microscope and a profilometer on the areas 816×816 μm, and three-dimensional images before and after the scratch tests, were obtained with the aid of a TalySur CCI Lite Taylor Hobson profilometer – from this changes of the root-mean- square (RMS) surface roughness resulting from scratching were found.

Spectral response of the optical fiber LPG sensors was investigated in the wavelength (λ) range of 1100 – 1700 nm using Yokogawa AQ6370B spectrum analyser and Leukos SM30 supercontinuum broadband light source. A schematic representation of the measurement setup for the optical transmission monitoring was presented elsewhere [65]. The LPG sensor was kept under constant mechanical and thermal conditions (at the ambient temperature approx. 20°C) during all the measurements. Stability of the ALD-deposited-oxide overlay of the sensor was investigated by multiple immersion of the sensor into the alkali solution and back into the DI water, and verification of the LPG spectral response at selected stages of this treatment (basically in DI water, because of higher sensibility of the sensor in this environment). The tested NaOH solutions had concentrations of 10 μM (pH 9) and 1 M. Such alkali-treatment durations were 5 min-lasting for pH 14 and 10 min-lasting for pH 9.

3. Results and discussion

3.1. Resistance of the planar oxide layers to alkali

The Hf_xO_y, Zr_xO_y and Ta_xO_y planar layers (with y/x of approx. 2.70, 2.07 and 2.75, respectively) proved to be stable even under the test of 20 h-lasting immersion in alkali having pH of 14. The thicknesses of the tested layers stayed unchanged with accuracy of the SE measurement, within the procedure described in Section 2.2. Such long-lasting stability of the Hf_xO_y layer may be found somewhat surprising - as this material has rather been suspected of being soluble in strong alkali (see the Introduction). The Al_2O_3 planar layers dissolve in alkali having pH of 14 with approximately constant rate approx. 4 nm/min, so the etching process was clearly observable already after 5 min-lasting immersion.

It should be explained here, that the bath duration of 20 h was chosen on an arbitrary basis. One should notice, however, that such test duration is much longer that an individual measurement done using sensor (which is a matter of minutes, rather). Therefore, the 20 h-lasting stability test, without observable etching, was found very reliable regarding the promising chemical properties of

the oxides. The 20 h stability in pH 14 informs also that the stability in more diluted alkali would be even longer.

3.2. Ellipsometry-based analyses of uniformity of the oxide layers and reproducibility of the ALD processes

The as-grown layers (Hf_xO_y, Ta_xO_y and Zr_xO_y) show monotonic horizontal gradient of thickness. The layers were the thickest at the vicinity of the gas inlet – so the closest to the Si quarter curved edge (see positioning the substrates in Section 2.1). The layers were growing thinner with the increasing distance from the gas inlet. Therefore, the thickness of each layer decreases monotonically in the direction of precursor gas flow. The layer thickness change (drop) in this direction over the approx. 2 in distance ($\Delta d_{2\ in}$) was measured for each layer. The percentage thickness drop over this distance was calculated as a ratio of $\Delta d_{2\ in}$ to the largest thickness at the sample (i.e., to the thickness close to the gas inlet, at the beginning of the 2 in distance). This percentage thickness drop was approx. 1.6%, 4.2% and 6.1% for the Hf_xO_y, Ta_xO_y and Zr_xO_y layer, respectively. It should be emphasized that the layer thickness gradient along the gas flow direction was not constant. It was rapidly decreasing with the distance. A visual correlation was also noticed - this rapid thickness decrease was observed already as a colour pattern of the sample surface. The percentage drop of the layer thickness at the sample centre (i.e., midway between the beginning and the end of the 2 in distance), $\Delta d_{1\ in}$, was 1.5% for Hf_xO_y, 3.2% for Ta_xO_y, and 4.1% for Zr_xO_y. From this it is seen that the relatively fastest drop was found for Hf_xO_y and the relatively slowest – for Zr_xO_y.

The finite uniformity of thickness of hafnium oxide and zirconium oxide layers deposited by LT-ALD has already been reported [66]. From these reports one can conclude, that the layer uniformity could be significantly improved. However, necessary is the expense of multiple increase of the neutral-gas purging durations, along with multiple increase of the overall process duration. For Ta_xO_y a very strong temperature dependence (increase of GPC with decreasing ALD-process temperature) has been observed around 100°C [67]. Therefore, the possible reason of the Ta_xO_y layer nonuniformity can be substrate-cooling effect generated by inlet gases. As such cooling is probably nonuniform over the sample surface it can result in the layer thickness gradient. Therefore, it can be concluded that the observed nonuniformity of the planar layers is generally a side-effect of LT-conditions of the ALD processes.

It should be noticed here, that in the case of optical fibers the surface temperature gradient and hence also the overlay thickness nonuniformity is likely mitigated. The reason is that their long axes were positioned perpendicularly to the direction of gas flow, and at the same time they were positioned relatively far from the gas inlet.

In contrast to the above discussed oxides for the Al_2O_3 layer the thickness gradient was not observed. The probable reason is that around 100°C the GPC of Al_2O_3 does not depend on ALD-process temperature. The lateral variation of the Al_2O_3 thickness was at the level of repeatability of the SE measurement for such layers (<0.1% of the nominal thickness value).

The *n* values were increasing with the layer thickness, with saturation of this trend around 100 nm. However, a weak dependence is seen already above approx. 50 nm (figure 1 a). For visible (VIS) and near infrared (NIR) radiation the highest *n* for such thickness range was obtained for Zr_xO_y and the lowest for Hf_xO_y (figure 1 b). The typical *n* values, measured at λ=632 nm, were approx. 2.00, 2.08 and 2.10 for Hf_xO_y, Ta_xO_y and Zr_xO_y layers, respectively. The EMA layers (the "surface roughness") fitted in the Zr_xO_y-related ellipsometric models had *n* values in the range 1.04-1.84. The *n*-value distribution shows uniformity over the surfaces. For some sample-surface sites lying close to gas inlet the *n* value was observed to be slightly higher (+ approx. 0.005) – that can be a simple result of thicker layer in this place.

The extinction coefficients were negligible in the full investigated spectral range.

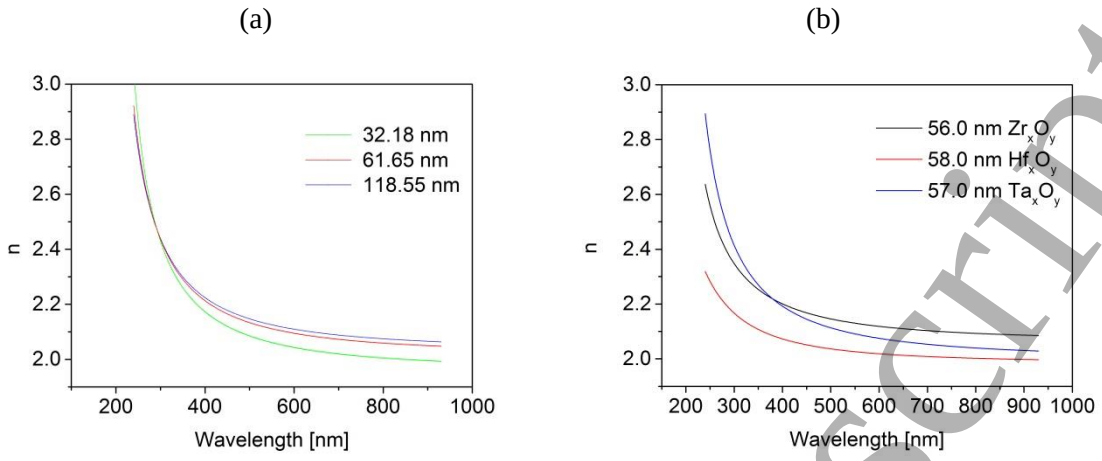

Figure 1. Wavelength-dependent *n* for Ta_xO_y layers with different thicknesses (a) and for Ta_xO_y, Zr_xO_y and Hf_xO_y layers with very similar thicknesses (b) deposited on Si and measured at the geometrically-comparable central positions of their surfaces.

Run-to-run GPC reproducibility of the ALD processes was best for Hf_xO_y (0.145±0.001 nm/cycle, that was comparable for Al_2O_3), and the poorest for Ta_xO_y (0.133±0.003 nm/cycle). The data assume normal distribution of GPC and 95% confidence interval for probes of over twenty processes per each type of oxide. The higher the GPC reproducibility, the higher the reproducibility of sensorial response of the fabricated device.

3.3. Structural and topographical properties of the oxide layers

The Hf_xO_y and Ta_xO_y layers deposited on glass proved to be fully amorphous, when analysed up to the thickness of approx. 200 nm (figure 2). Also the approx. 50 nm-thick Zr_xO_y layers were found fully amorphous. In contrary to this, the approx. 200 nm-thick Zr_xO_y layers had already apparent contribution of crystallinity, although they were predominantly amorphous (figure 2). Namely, the XRD signals positioned at 2 *theta* angle of approx. 35.598° and of approx. 60.460° are probably responsible for diffraction on ZrO_2 tetragonal phase – on (110) plane and (211) plane, respectively [68]. As a reference, it can be mentioned that the degree of crystallinity of approx. 10% has already been reported for 100 nm-thick ZrO_2 ALD-deposited at the temperature 100°C [69]. However, because of very small XRD signals for our approx. 200 nm-thick Zr_xO_y it was impossible to determine in quantitative terms the degree of its crystallinity. Anyway, we assume that in our Zr_xO_y very small stoichiometric ZrO_2 grains are embedded in the mostly amorphous (and not stoichiometric) layer, which average composition stays approx. $ZrO_{2.07}$.

The amorphousness of the layers is likely to contribute to their increased surface smoothness, in comparison with polycrystalline forms. Hence, it also helps to maintain the strict uniformity of the layer thickness. Amorphousness is also a prerequisite of layer tightness as well as higher chemical resistance in comparison with polycrystalline forms. This results from the fact that boundaries of crystalline grains are less thermodynamically stable "weak points" of the polycrystalline layers. The amorphous growth was, again, an advantage of LT-conditions of the ALD process.

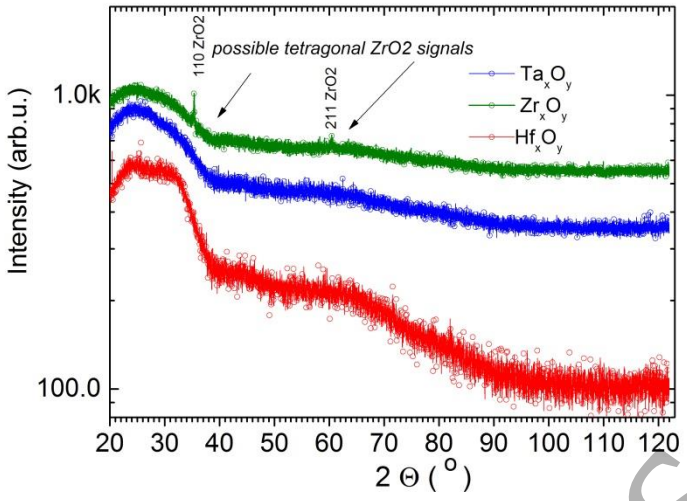

Figure 2. XRD 2 *theta-omega* scan profiles for ~200 nm-thick Hf_xO_y, Zr_xO_y and Ta_xO_y layers (with y/x approx. 2.70, 2.07 and 2.75, respectively) deposited on glass. The Zr_xO_y composition was slightly overstoichiometric and the oxide was mostly amorphous. However, there are also clearly seen two small signals that can be interpreted as belonging to the stoichiometric ZrO_2 tetragonal crystallites (for 110 and 211 orientations). The crystallites must have been very small – the most probably they have nanometre-scale sizes. The other narrow lines seen in the profiles were found to be noise only. The glass substrates were non-qualified in terms of their structural properties, and this may be the reason of the observed differences for the above presented diffractograms for 2 *theta* angles below 35°.

The layers had granular surface topographies. The RMS surface roughness was typically ~0.5 nm at the area of 10×10 μm^2 and was slightly higher for the layers deposited on glass than for the layers on Si. This can be a simple result of influence of the initial substrate topography - for comparison, the typical RMS surface roughness for the bare Si wafers and bare glass plates was ~0.1 and ~1 nm, respectively. The AFM-measured surface roughness of the oxide layers was typically less than ~1% of the oxide layer thickness. Figure 3 presents the respective AFM images with quite similar surface topography for two different oxides.

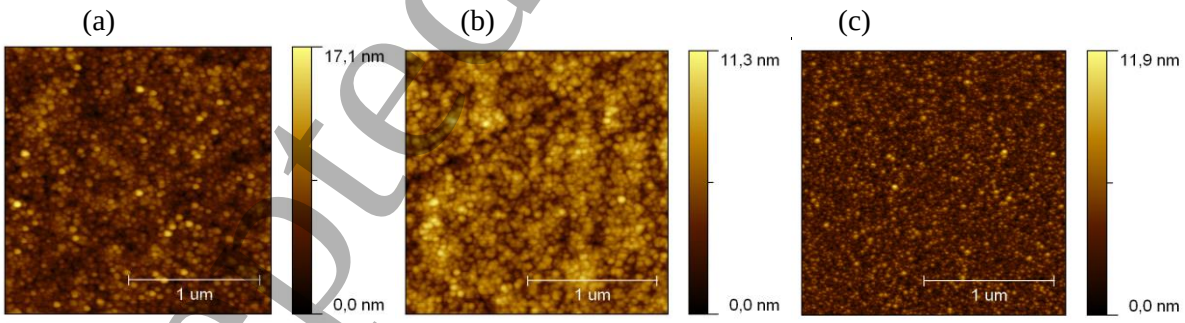

Figure 3. Atomic force microscopic images obtained for the layers grown on glass. The 2x2 μm^2 areas were scanned for the surface of 51.5 nm-thick Zr_xO_y layer (a) 59.5 nm-thick Ta_xO_y layer (b) and 58.5 nm-thick Hf_xO_y layer (c). Only few several-nanometre-high particles are present on the surfaces – likely being the nonintentional result of the sample cleaving.

The AFM method showed that all the analysed layers had very similar surface roughness. It should be noticed, however, that the SE of the Zr_xO_y-related samples required assumption of a surface roughness (i.e., with the mentioned earlier EMA layer) in a fitted model of the structure. This, in turn, indicates that their surface roughness was more pronounced than for the Ta_xO_y and Hf_xO_y layers. The possible explanation of this difference between SE and AFM-based results for Zr_xO_y layers is the

limited resolution of AFM, when it comes to imaging of deep and narrow surface slits, that are perhaps present at the Zr_xO_y surface. The rougher surface of Zr_xO_y detected by SE can be a result of some crystallinity being the confirmed issue of Zr_xO_y.

3.4. Tribological properties of the oxide layers

The H_{it} and E_{it} of the layers are presented in table 1. For comparison, the H_{it} and E_{it} of the bare glass substrate are about 6.50-6.75 GPa and 60-65 GPa, respectively, while the E_{it} of a silica fiber is approx. 73 GPa. It can be noticed, that the differences of mechanical properties of glass and of the oxides are not very large. Anyway, the Zr_xO_y layers were harder than the Hf_xO_y and Ta_xO_y layers and even harder than the glass substrate. The Hf_xO_y and Ta_xO_y layers were slightly softer than the glass. The nanohardness of the ALD-deposited layers was roughly similar that of conventional-magnetron-sputtered TiO_2 thin layers, for example, which often used to be used for optical coatings [70]. The layers were also slightly less elastic than the glass, and the Zr_xO_y layer was the most stiff. The results of the H_{it} and E_{it} measurements is shown in figure 4.

Table 1. Nanohardness and Young moduli for the ALD ~200 μm-thick oxide layers grown on glass

Sample	H_{it} [GPa]	E_{it} [GPa]
Hf_xO_y/glass	4.95 ± 0.60	83.7 ± 11.7
Ta_xO_y /glass	4.90 ± 0.20	92.9 ± 4.9
Zr_xO_y/glass	8.64 ± 0.16	104.4 ± 10.8

(a) (b)

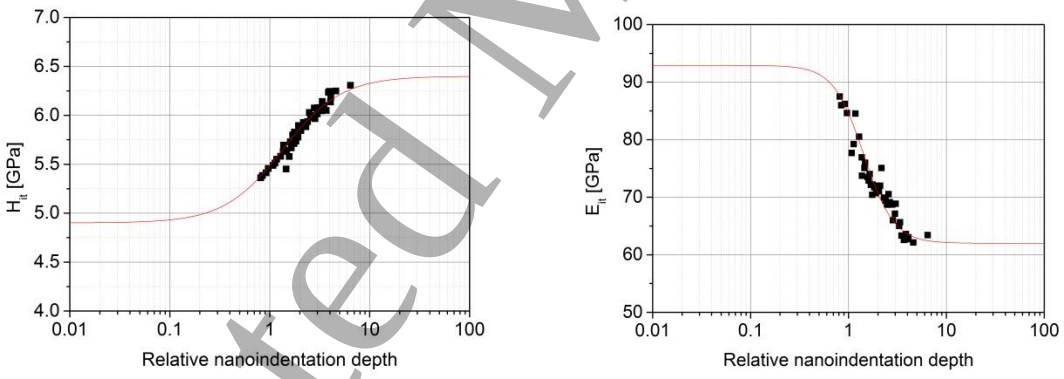

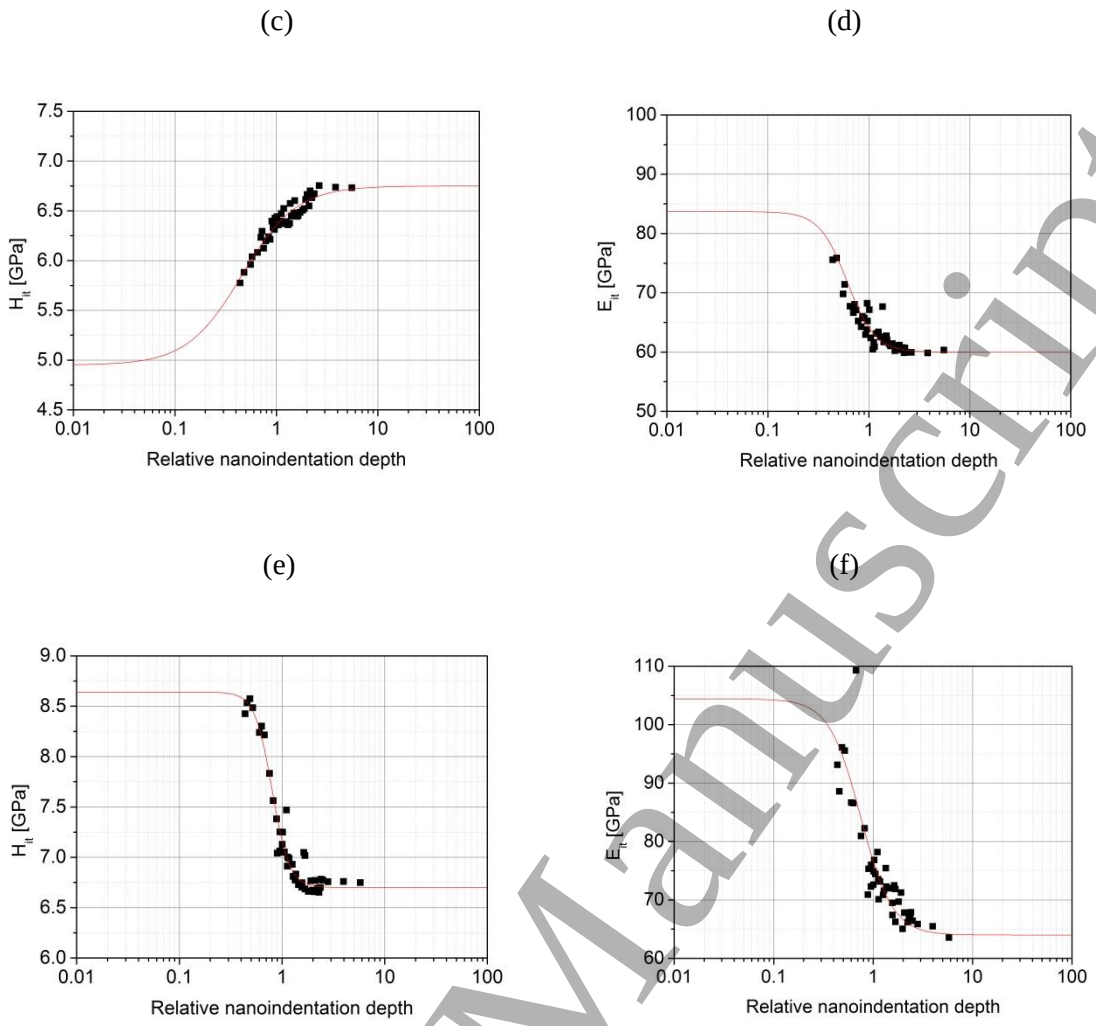

Figure 4. Nanohardness (a, c, e) and Young's modules (b, d, f) of the approx. 200 nm-thick oxide layers deposited on glass: Ta_xO_y (a, b), Hf_xO_y (c, d), Zr_xO_y (e, f). The relative nanoindentation depth is defined as $h/d \times 100\%$, where h is the maximum indenter displacement and d is the thickness of the thin film. The measured values are marked as black points, while solid curves through data points represent simultaneous regression best fits to each data set.

Relative changes of RMS surface roughness being the result of the performed scratch tests are presented in table 2. According to these data, the Hf_xO_y and Ta_xO_y layers proved to be significantly more scratch resistant than the Zr_xO_y one.

Table 2. Calculated relative increase of RMS surface roughness being the result of scratching (the percentage of difference between the resulting and initial roughness divided by the initial RMS value)

Sample	Relative RMS surface roughness increase (%)
Hf_xO_y/glass	20
Ta_xO_y /glass	33
Zr_xO_y/glass	230

It should be noted that overlay harder than the silica fiber itself (Zr_xO_y in this case), allow for better protection of the fiber sensor against compressive damage, that may be caused by pinching or

clamping the fiber. On the other hand the higher scratch resistance of the Hf_xO_y and Ta_xO_y allows them for better protection of the fiber against abrasive damage, that can be caused by a sliding contact with a sharp object or jagged surfaces. Higher elasticities (particularly for the Hf_xO_y, the most similar to silica) can be an advantage, as they suppress the vulnerability of the overlay on tensile stress, that can be caused by straight tension, bending or torsion of the fiber. The better protection against compressive damage, tensile stress and scratching helps to reduce the risk of cracking, splitting or delamination of the overlay.

3.5. Hydrophilic properties of the oxide surfaces

The oxide overlays are elaborated for use in biosensors. These are fabricated using functionalisation process of the overlay [71, 72]. By this process their selective operation targeted for given analyte is initialised. The most often the surface functionalisation is based on silanization process. For this, the presence of hydrophilic functional groups (the most often hydroxyl groups) at the overlay surface is necessary. Therefore, the increasing hydrophilicity of the oxide surface increases efficiency of the silanization process (and hence, also the functionalisation efficiency). Therefore it is an advantageous feature of the oxide surface.

The water contact angles for the layers presented in table 3 are below 90º that indicates hydrophilic properties of the layers. The most hydrophilic was the surface of Zr_xO_y layers and the less hydrophilic was the Ta_xO_y surface.

Table 3. Wetting angles for DI water on the surface of the layers deposited on glass

Layer	Wetting angle
Hf_xO_y	59.4±1.7º
Ta_xO_y	62.9±1.2º
Zr_xO_y	52.5±1.5º

3.6. Resistance of the long period grating optical fiber sensor overlaid with the Ta_xO_y to alkali

The Ta_xO_y overlays were deposited on LPG optical fibers. The choice of the concrete type of oxide for overlay fabrication was done on an arbitrary basis. However, it should be indicated that the following set of characteristics of Ta_xO_y was found as its valuable competitive advantage: chemical resistance in alkali, amorphousness, relatively high *n* value, and high surface smoothness. The transmission spectral response lines for a set of LPG optical fiber sensors are presented in figure 5. The respective measurements were performed in DI water (which refractive index is n_D~1.3330 RIU). The optimum overlay thickness ensuring the maximum sensitivity of such a sensor to the overlay thickness was found to be close to 63.6 nm, when the sensor is immersed in DI water. A pair of resonances is seen at λ~1401 nm and λ~1533 nm. Their depths and their spectral separation increase with increasing overlay thickness. It is seen that the sensor is sensitive to nm-level changes of the Ta_xO_y overlay thickness. The longer-wavelength resonance of the sensor exhibits higher sensitivity to the overlay thickness, than the shorter-wavelength resonance.

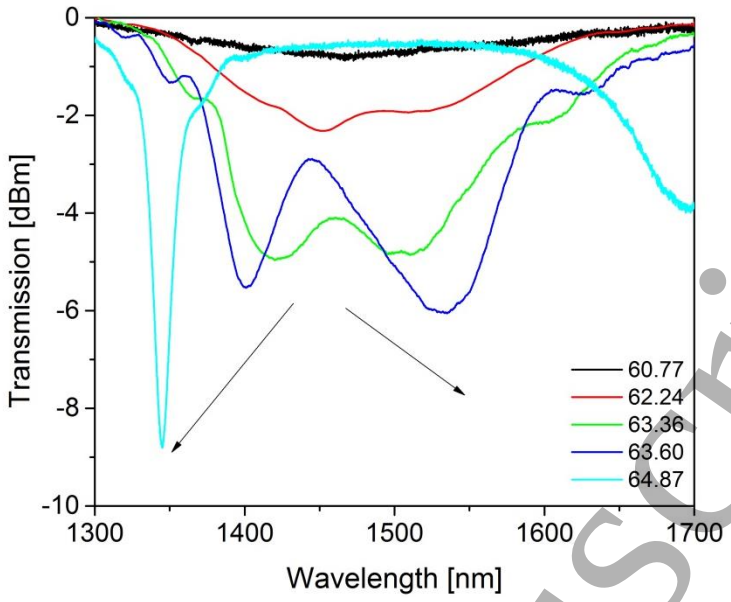

Figure 5. Transmission spectral response lines for a set of LPG-optical-fiber sensors overlaid by Ta_xO_y with various thicknesses between 60.77 nm to 64.87 nm, immersed in DI water. The arrows indicate direction of changes of position and depth of the resonance minima for the increasing overlay thickness.

In figure 6 the transmission spectral response lines are presented for an individual LPG-optical-fiber sensor with the initially 64.87 nm-thick Ta_xO_y overlay. The measurements were performed sequentially in DI water and in 1 M NaOH solution (pH 14). Because of different n values of DI water and 1 M NaOH solution (which refractive index is $n_{1M\ NaOH\ aq} > n_D$) the respective initial transmission resonances were observed in these two environments for different wavelengths. The initial most prominent DI-water-related resonances were observed at $\lambda \sim 1238.5$ nm, $\lambda \sim 1341$ nm and $\lambda > 1700$ nm. The sensor was consecutively immersed in water-alkali-water-alkali-water sequence, with the two 5 min-lasting immersions in alkali. For the overlay thickness applied here, the sensitivity to overlay thickness changes is much higher for the sensor being immersed in DI water than when it is immersed in the alkali. Therefore the measurements taking place in DI water allow for more reliable monitoring of the actual overlay thickness – and they do show the successive loss of overlay thickness that we interpret as being the result of its etching in alkali.

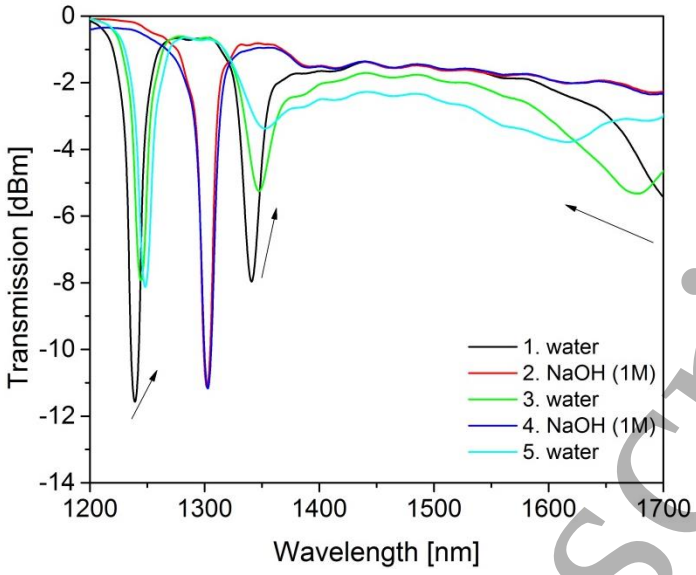

Figure 6. Transmission spectral response lines obtained in a series of consecutive measurements performed sequentially in DI water and NaOH solution with pH 14 for an individual LPG-optical-fiber sensor overlaid with the initially 64.87 nm-thick Ta_xO_y. The arrows indicate direction of changes of position and depth of the resonance minima for the consecutive measurements done in DI water.

With the assistance of linear fits relating to the dependencies of the resonant wavelengths on the Ta_xO_y overlay thickness, which are seen in figure 7, the possible overlay loss being the result of the sensor immersion in 1 M NaOH solution was estimated. Its value is in the range 0.25-0.63 nm. The calculated on this basis mean etching rate of the Ta_xO_y overlay in alkali was 0.025-0.063 nm/min, which was still much slower than the earlier observed etching for the similar sensor overlaid with ALD-deposited Al_2O_3 instead of Ta_xO_y (the observed Al_2O_3 etching rate in 10 mM NaOH solution was approx. 1.78 nm/min [73]). The exact dynamics of the Ta_xO_y overlay etching process is not known. In particular it is not clear if the etching rate slowed down over the course of immersion in alkali. The reason why is the Ta_xO_y overlay deposited on the fiber less alkali resistant, than the planar layer deposited in the same conditions, is also not clear and needs further study. A hypothetical explanation could be that there is a difference of surface properties of Ta_xO_y deposited on Si wafer and on the fiber, in terms of O/Ta atomic ratio or possible contamination.

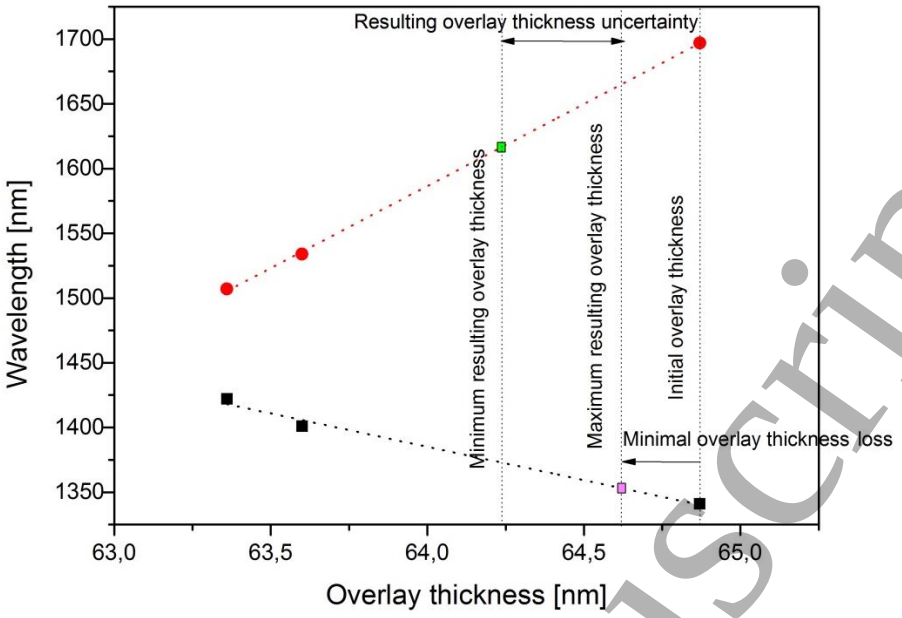

Figure 7. The experimental dependencies of the resonant wavelengths on the Ta_xO_y overlay thickness - data extracted from the measurements presented in figure 5 for the shorter wavelength left-hand-side resonance minima (black squares) and for the longer wavelength right-hand-side resonance minima (red circles). The linear regressions of these dependencies, being a simplification, are presented by respective dotted straight lines. The small coloured squares are positioned on these lines at the respective resonant wavelengths measured for the sensor immersed in DI H_2O after the 5 min+5 min-lasting immersion in 1 M NaOH solution (corresponding to the minima of the line number 5 in figure 6).

Furthermore, for the individual Ta_xO_y-overlaid LPG-based optical fiber sensor the transmission spectral response measurements were performed sequentially in DI water and in 10 μM NaOH solution (pH 9). Again, the sensor was consecutively immersed in water-alkali-water-alkali-water sequence, this time with the two 10 min-lasting immersions in alkali. Because of very similar *n* values of DI water and 10 μM NaOH solution the respective transmission resonances were observed in these two environments for nearly the same wavelengths. What should be emphasized here, the virtual stability of their positions observed during the whole experiment confirmed the chemical stability of the Ta_xO_y overlay in alkaline environment with pH 9. The described measurements were performed repeatedly with reproducible result.

4. Summary and conclusions

The planar layers of Hf_xO_y, Ta_xO_y and Zr_xO_y deposited by LT (100°C) ALD have proved their long-lasting chemical stability in harsh alkaline environment with pH 14. Therefore the oxides proved they had high potential as materials for alkali-resistant overlays of optical sensors. The LT-deposition was safe for the thermally-vulnerable sensors. It should be noticed here that in the case of optical fibers the surface temperature gradient (a drawback of LT ALD conditions) and hence also the overlay thickness nonuniformity is very likely mitigated because of their small diameter – despite observation of the thickness gradients for the planar test samples.

Though the pH 14-bath duration of 20 h was chosen on an arbitrary basis it is obvious, that such test duration is much longer that an individual measurement done using sensor (which is a matter of minutes, rather). Therefore, the 20 h-lasting stability test, without observable etching, was found very reliable regarding the promising chemical properties of the oxides.

Numerous analyses revealed strengths and weaknesses of the given ALD-deposited oxide regarding its applicability for the optical sensor overlay.

All the examined oxides have their specific advantages and drawbacks. Therefore, the choice of the Ta_xO_y for overlay fabrication was done on an arbitrary basis. The strong point of Ta_xO_y is high surface smoothness together with complete amorphousness, high scratch resistance, and relatively high value of *n*. Amorphousness of the Ta_xO_y contributes to the high surface smoothness of the layers and is also a prerequisite of layer tightness and its chemical resistance. The high scratch resistance of Ta_xO_y is a prerequisite of better protection of the fiber against abrasive damage, in comparison with Zr_xO_y. Relatively high *n* of Ta_xO_y allows for deposition LPG-sensor overlays by approx. 10% thinner than in the case of Hf_xO_y.

The drawback of Ta_xO_y is relatively low run-to-run reproducibility of GPC in ALD process. This results in relatively large distribution of the deposited layers/overlays within a series of ALD processes. It should be emphasized, however, that it still does not hinder successful manufacturing of the LPG sensors, though it decreases yield in a series of deposition processes.

The advantages of Hf_xO_y are: high lateral uniformity of the layers, high surface smoothness together with complete amorphousness, high elasticity, high scratch resistance, high facility of SE-based control, relatively high value of GPC, and high run-to-run reproducibility of GPC in ALD process. The relatively low values of *n* and nanohardness are its drawbacks. The advantages of Zr_xO_y stem from high *n*, high nanohardness, and high value of GPC. Its drawbacks are low lateral uniformity of the layers, low surface smoothness together with only partial amorphousness, low elasticity, low scratch resistance and low facility of SE-based control, which accuracy suffers from surface roughness. The properties of the thin oxides are compared in quantitative terms in table 4, summarizing the research results.

Table 4. Comparison of properties of the analysed thin oxides; the minus sign means lack of data

LPG OFS overlay property	Hf_xO_y	Ta_xO_y	Zr_xO_y	Al_2O_3
chemical resistance in pH 14	-	etching 0.025-0.063 nm/min	-	-
chemical resistance in pH 9	-	etching not observed	-	etching approx. 1.78 nm/min [73]

Planar layer property	Hf_xO_y	Ta_xO_y	Zr_xO_y	Al_2O_3
chemical resistance in pH=14	etching not observed	etching not observed	etching not observed	etching approx. 4 nm/min
lateral nonuniformity @ 2 in distance (see Section 3.2)	approx. 1.6% (thickn. gradient)	approx. 4.2% (thickn. gradient)	approx. 6.1% (thickn. gradient)	no thickness gradient
n value (@ λ=632 nm)	approx. 2.00	approx. 2.08	approx. 2.10	approx. 1.62
amorphousness	complete	complete	partially polycrystalline	complete
surface roughness - by AFM (RMS (nm)@10x10 μm^2)	approx. 0.5	approx. 0.5	approx. 0.5	< 0.5

- by SE (EMA surface layer)	w/o	w/o	≤ 10% of nominal layer thickness	w/o
nanohardness [GPa]	4.95 ± 0.60	4.90 ± 0.20	8.64 ± 0.16	-
Young modulus [GPa]	83.7 ± 11.7	92.9 ± 4.9	104.4 ± 10.8	-
scratch resistance - relative RMS surf. rough. increase (%)	20	33	230	-
hydrophilicity – wetting angle in DI H_2O	59.4±1.7º	62.9±1.2º	52.5±1.5º	-
facility of SE-based control	very high ($\chi^2 \leq 0.5$)	high ($\chi^2 \leq 1$)	low (due to surf. rough.)	very high ($\chi^2 \leq 0.5$)
GPC (nm/cycle)	0.145	0.133	0.150	0.099
run-to-run GPC reproducibility (nm/cycle)	±0.001	±0.003	±0.002	±0.001
growth rate (nm/s)	0.021	0.019	0.022	0.020

The Ta_xO_y overlay deposited on optical fibers with induced LPGs resulted in resistance of such fibers to alkali with pH 9, which used to be used as a chemical agent for regeneration of biosensor with silane-functionalized surface. Thereby, such optical fiber biosensors overlaid by the ALD-deposited Ta_xO_y have a potential to be regenerable and repeatedly reused. Surprisingly, it was found that harsh alkali (pH 14) dissolves the Ta_xO_y overlays with the approximate rate of 0.025-0.063 nm/min. Why the chemical stability in harsh alkali of the Ta_xO_y overlay deposited on fiber differs with respect to the Ta_xO_y planar layer is still not clear, and needs further research. However, it is worth mentioning the Ta_xO_y overlays are still much more durable in alkali than Al_2O_3 overlays that are often used in optical sensors.

Acknowledgments:

The work was financially supported as statutory activities at the Instytut Technologii Elektronowej and by National Science Center in Poland under grant No. 2011/03/D/NZ7/02054.

Iga Ścislewska's experimental work has taken place during her student internship at the Instytut Technologii Elektronowej.

References:

[1] Ishaq I M, Quintela A, James S W, Ashwell G J, Lopez-Higuera J M, Tatam R P 2005 Modification of the refractive index response of long period gratings using thin film overlays *Sensors and Actuators B: Chemical* 107(2) 738-741.

[2] Lee B 2003 Invited paper: Review of the present status of optical fiber sensors *Optical Fiber Technology* 9(2) 57-79

[3] Grattan K T V and Sun T 2000 Fiber optic sensor technology: an overview *Sensors and Actuators A: Physical* 82(1) 40-61
[4] Gouveia C A J, Baptista J M, Jorge P A S 2013 Chapter 13. Refractometric Optical Fiber Platforms for Label Free Sensing *Current Developments in Optical Fiber Technology* Edited by Sulaiman Wadi Harun and Hamzah Arof Publisher: InTech
[5] Paliwal N and John J 2015 Lossy mode resonance (LMR) based fiber optic sensors: A review *IEEE Sensors Journal* 15(10) 5361-5371
[6] Arregui F J et al. 2014 Fiber-Optic Lossy Mode Resonance Sensors, *Procedia Engineering* 87 EUROSENSORS 2014, the XXVIII edition of the conference series 3 – 8
[7] Greenwood N N and Earnshaw A 1984 *Chemistry of the Elements* Pergamon Press; Oxford (UK) 393-99
[8] https://www.google.ch/patents/US20090103084
[9] Dominik M, Niedziółka-Jönsson J, Roźniecka E, Wachnicki Ł, Godlewski M, Mikulic P, Bock W J, Śmietana M 2016 Regeneration of titanium oxide nano-coated long-period grating biosensor *Sixth European Workshop on Optical Fibre Sensors* (Vol. 9916, p. 99160Z) International Society for Optics and Photonics.
[10] Dominik M, Leśniewski A, Janczuk M, Niedziółka-Jönsson J, Hołdyński M, Wachnicki Ł, Godlewski M, Bock W J, Śmietana M 2017 Titanium oxide thin films obtained with physical and chemical vapour deposition methods for optical biosensing purposes *Biosensors and Bioelectronics* 93 102-109
[11] El-Shamy T M and Pantano C G 1977 Decomposition of silicate glasses in alkaline solutions *Nature* 266 704-706
[12] Zhu S, Pang F, Huang S, Zou F, Dong Y, Wang T 2015 High sensitivity refractive index sensor based on adiabatic tapered optical fiber deposited with nanofilm by ALD *Optics Express* 23(11) 13880-13888
[13] Hernáez M, Del Villar I, Zamarreño C R, Arregui F J, Matias I R 2010 Optical fiber refractometers based on lossy mode resonances supported by TiO2 coatings *Applied Optics* 49(20) 3980-3985
[14] Zhu S, Pang F, Huang S, Zou F, Guo Q, Wen J, Wang T 2016 High sensitivity refractometer based on TiO2-coated adiabatic tapered optical fiber via ALD technology *Sensors* 16(8) 1295
[15] Sanchez P, Zamarreno C R, Zamarreo C R, Hernaez M, Matias I R, Arregui F J 2014 Exhaled breath optical fiber sensor based on LMRs for respiration monitoring *SENSORS, 2014 IEEE* 1142-1145
[16] Del Villar I, Zamarreño C R, Sanchez P, Hernaez M, Valdivielso C F, Arregui F J, Matias I R 2010 Generation of lossy mode resonances by deposition of high-refractive-index coatings on uncladded multimode optical fibers *Journal of Optics* 12(9) 095503
[17] Del Villar I, Zamarreño C R, Hernaez M, Arregui F J, Matias I R 2010 Lossy mode resonance generation with indium-tin-oxide-coated optical fibers for sensing applications *Journal of Lightwave Technology* 28(1) 111-117.
[18] Zamarreño C R, Hernaez M, Del Villar I, Matias I R, Arregui F J 2010 Tunable humidity sensor based on ITO-coated optical fiber *Sensors and Actuators B: Chemical* 146(1) 414-417
[19] Kaur D, Sharma V K, Kapoor A 2014 High sensitivity lossy mode resonance sensors *Sensors and Actuators B: Chemical* 198 366-376
[20] Zamarreño C R, Lopez S, Hernaez M, Del Villar I, Matias I R, Arregui F J 2012 Resonance-based refractometric response of cladding-removed optical fibers with sputtered indium tin oxide coatings *Sensors and Actuators B: Chemical* 175 106-110
[21] Zubiate P, Zamarreño C R, Del Villar I, Matias I R, Arregui F J 2015 High sensitive refractometers based on lossy mode resonances (LMRs) supported by ITO coated D-shaped optical fibers *Optics Express* 23(6) 8045-8050
[22] http://www.indium.com/ Indium Corporation® Application Note, Indium Oxide and Indium-Tin Oxide (ITO) Coatings
[23] Socorro A B, Del Villar I, Corres J M, Arregui F J, Matias I R 2014 Spectral width reduction in lossy mode resonance-based sensors by means of tapered optical fibre structures *Sensors and Actuators B: Chemical* 200 53-60

[24] Beavon R and Jarvis A 2003 *Periodicity, Quantitative Equilibrium and Functional Group Chemistry* Nelson Thornes 19
[25] S. Chands Success Guide (Q&A) Inorganic Chemistry, Gaurav Madan, p. 604
[26] Leamy D and Regan F 2003 A robust spin-coated optical sensing device for rapid determination of predominant metal ions in wastewater streams *International Journal of Environmental & Analytical Chemistry* 83(10) 867-877
[27] Korent Š M, Lobnik A, Mohr G J 2007 Sol-gel-based optical sensor for the detection of aqueous amines *Analytical and bioanalytical chemistry* 387(8) 2863-2870
[28] Shao L Y, Yin M J, Tam H Y, Albert J 2013 Fiber optic pH sensor with self-assembled polymer multilayer nanocoatings *Sensors* 13(2) 1425-1434
[29] Bogdanowicz R, Śmietana M, Gnyba M, Gołunski Ł, Ryl J, Garda M 2014 Optical and structural properties of polycrystalline CVD diamond films grown on fused silica optical fibres pre-treated by high-power sonication seeding *Applied Physics A* 116(4) 1927-1937
[30] Xie W, Yang M, Cheng Y, Li D, Zhang Y, Zhuang Z 2014 Optical fiber relative-humidity sensor with evaporated dielectric coatings on fiber end-face *Optical Fiber Technology* 20(4) 314-319
[31] Schmitt K, Oehse K, Sulz G, Hoffmann C 2008 Evanescent field sensors based on tantalum pentoxide waveguides–a review *Sensors* 8 711-738
[32] Johnson R W, Hultqvist A, Bent S F 2014 A brief review of atomic layer deposition: from fundamentals to applications *Materials Today* 17(5) 236-246
[33] Raaijmakers I J 2011 Current and future applications of ALD in micro-electronics *ECS Transactions* 41(2) 3-17
[34] Kim H 2003 Atomic layer deposition of metal and nitride thin films: Current research efforts and applications for semiconductor device processing. *Journal of Vacuum Science & Technology B: Microelectronics and Nanometer Structures Processing, Measurement, and Phenomena* 21(6) 2231-2261
[35] Im H, Wittenberg N J, Lindquist N C, Oh S H 2012 Atomic layer deposition (ALD): A versatile technique for plasmonics and nanobiotechnology *Journal of Materials Research*, 27(4), 663-671
[36] Godlewski M, Gierałtowska S, Wachnicki Ł, Pietuszka R, Witkowski B S, Słońska A, Gajewski Z, Godlewski M M 2017 High-k oxides by atomic layer deposition-Applications in biology and medicine *Journal of Vacuum Science & Technology A: Vacuum, Surfaces, and Films* 35(2) 021508
[37] Śmietana M, Myśliwiec M, Mikulic P, Witkowski B S, Bock W J 2013 Capability for fine tuning of the refractive index sensing properties of long-period gratings by atomic layer deposited Al2O3 overlays *Sensors* 13(12) 16372-16383
[38] Zhao Y, Pang F, Dong Y, Wen J, Chen Z, Wang T 2013 Refractive index sensitivity enhancement of optical fiber cladding mode by depositing nanofilm via ALD technology *Optics Express* 21(22) 26136-26143
[39] Purniawan A, Pandraud G, Moh T S Y, Marthen A, Vakalopoulos K A, French P J, Sarro P M 2012 Fabrication and optical measurements of a TiO2-ALD evanescent waveguide sensor *Sensors and Actuators A: Physical* 188 127-132
[40] Śmietana M, Koba M, Mikulic P, Bock W J 2016 Towards refractive index sensitivity of long-period gratings at level of tens of μm per refractive index unit: fiber cladding etching and nano-coating deposition *Optics Express* 24(11) 11897-11904
[41] Awaludin Z, Okajima T, Ohsaka T 2014 Preparation of reduced tantalum pentoxide by electrochemical technique for oxygen reduction reaction *Journal of Power Sources* 268 728-732
[42] Morant C, Galan L, Sanz J M 1990 An XPS study of the initial stages of oxidation of hafnium *Surface and Interface Analysis* 16(1-12) 304–308
[43] Kuzmichev D S, Lebedinskii YuYu 2017 Resistive switching in MIM structure based on overstoichiometric tantalum oxide *Microelectronic Engineering* 178 150–153
[44] Wilk G D, Wallace R M, Anthony J M 2001 High-κ gate dielectrics: Current status and materials properties considerations *Journal of Applied Physics* 89 5243
[45] Anil K Mukherji Analytical Chemistry of Zirconium and Hafnium International in Series of Monographs in Analytical Chemistry Vol. 40 Publisher: Pergamon Press
[46] Namur R S, Reyes K M, Marino C E B 2015 Growth and Electrochemical Stability of Compact Tantalum Oxides Obtained in Different Electrolytes for Biomedical Applications *Materials Research* 18(2) 91-97

[47] Atanassova E, Aygun G, Turan R, Babeva T 2006 Structural and optical characteristics of tantalum oxide grown by pulsed Nd:YAG laser oxidation *J. Vac.Sci. Technol. A* 24(2) 206-211
[48] Huang A P, Yang Z C, Chu P K 2010 Hafnium-based High-k Gate Dielectrics *Advances in solid state circuit technologies* Edited by Paul K. Chu Publisher: InTech
[49] Misra D, Iwai H, Wong H 2005 High-k Gate Dielectrics *Interface* 14(2) 30-34
[50] Li X, Shao Y, Yu Y, Zhang Y, Wei S 2016 A highly sensitive fiber-optic Fabry–Perot interferometer based on internal reflection mirrors for refractive index measurement *Sensors* 16(6) 794
[51] http://www.reade.com/products/hafnium-oxide-powder-hfo2
[52] Srivastava V M and Singh G 2014 *MOSFET technologies for double-pole four-throw radio-frequency switch* Springer International Publishing 144
[53] Yu M et al. 2016 Novel vertical 3D structure of TaOx-based RRAM with self-localized switching region by sidewall electrode oxidation *Scientific Reports* 6 21020.
[54] http://tantalum.atomistry.com/tantalum_pentoxide.html
[55] Goldstein D N, McCormick J A, George S M 2008 Al2O3 Atomic Layer Deposition with Trimethylaluminum and Ozone Studied by in Situ Transmission FTIR Spectroscopy and Quadrupole Mass Spectrometry *J. Phys. Chem. C* 112 19530–19539
[56] Puurunen R L 2005 Surface chemistry of atomic layer deposition: A case study for the trimethylaluminum/water process *Journal of Applied Physics* 97 121301
[57] https://beneq.com/en/thin-films/products/atomic-layer-deposition/beneq-tfs-200
[58] Fujiwara H Spectroscopic Ellipsometry Principles and Applications Publisher: John Wiley & Sons
[59] Kwok D Y and Neumann A W 1999 Contact angle measurement and contact angle interpretation *Advances in colloid and interface science* 81(3) 167-249
[60] Oliver W C and Pharr G M 1992 An improved technique for determining hardness and elastic modulus using load and displacement sensing indentation experiments *Journal of Materials Research* 7(6) 1564-1583
[61] Fischer Cripps A C 2002 *Nanoindentation* Springer New York
[62] Martyniuk M, Antoszewski J, Walmsley B A, Musca C A, Dell J M, Jung Y-G, Lawn B R, Huang H, Faraone L 2005 Determination of mechanical properties of silicon nitride thin films using nanoindentation *Proc. of SPIE* vol. 5798 216-222
[63] ISO/TC 172/SC 7/WG 3 N30 Standard, Spectacle lenses – Test method for abrasion resistance1998.
[64] Blacker R, Bohling D, Coda M, Kolosey M, Marechal N 2000 Development of intrinsically conductive antireflection coatings for the ophthalmic industry. *Proceedings of The Annual Technical Conference-Society Of Vacuum Coaters* 212-216
[65] Koba M, Śmietana M, Brzozowska E, Górska S, Mikulic P 2015 Reusable Bacteriophage Adhesin-Coated Long-Period Grating Sensor for Bacterial Lipopolysaccharide Recognition *Journal of Lightwave Technology* 33(12)
[66] Hausmann D M, Kim E, Becker J, Gordon R G 2002 Atomic Layer Deposition of Hafnium and Zirconium Oxides Using Metal Amide Precursors *Chemistry of materials* 14(10) 4350-4358
[67] Kukli K, Aarik J, Aidla A, Kohan O, Uustare T, Sammelselg V 1995 Properties of tantalum oxide thin films grown by atomic layer deposition *Thin Solid Films* 260(2) 135-142
[68] The International Centre for Diffraction Data – ICDD (http://www.icdd.com/) reference code: 00-002-0733
[69] Hausmann D M and Gordon R G 2003 Surface morphology and crystallinity control in the atomic layer deposition (ALD) of hafnium and zirconium oxide thin films *Journal of Crystal Growth* 249(1) 251-261
[70] Wojcieszak D, Mazur M, Indyka J, Jurkowska A, Kalisz M, Domanowski P, Kaczmarek D, Domaradzki J 2015 Mechanical and structural properties of titanium dioxide deposited by innovative magnetron sputtering process *Materials Science-Poland* 33(3) 660-668
[71] Szunerits S, Shalabney A, Boukherroub R, Abdulhalim I 2011 Dielectric coated plasmonic interfaces: their interest for sensitive sensing of analyte-ligand interactions *Reviews in Analytical Chemistry* 31(1) 15–28
[72] Szunerits S, Boukherroub R 2012 Sensing using localised surface plasmon resonance sensors *Chem. Commun.* 48 8999–9010

[73] Śmietana M, Mikulic P, Bock W J 2018 Nano-coated long-period gratings for detection of sub-nanometric changes in thin-film thickness, *Sensors and Actuators A* 270 79-83